Geomechanics and Engineering, *Vol. 42, No. 1 (2025) 67-80*
https://doi.org/10.12989/gae.2025.42.1.067

Characteristics and mechanism of deterioration of tensile properties of coal samples under the action of pressure water immersion duration

Yizhen Zhang[1], Dawei Yin*[2], Pengxiang Sun[2], Shirui Zhang[3] and Yisong Ding[2]

[1]*Taiyuan Design Research Institute for Coal Industry, Taiyuan, China*
[2]*College of Energy and Mining Engineering, Shandong University of Science and Technology, Qingdao, China*
[3]*Shanxi Pulongwan Coal Industry Co., Ltd., Datong 034400, China*

(*Received August 8, 2024, Revised June 20, 2025, Accepted June 23, 2025*)

Abstract. Using a self-developed coal rock pressure water immersion test device, Brazilian splitting tests were performed on five sets of coal samples under dry and 3, 6, 9, and 12 months pressure water immersion duration (immersion pressure of 5 MPa) to study the tensile properties of coal rock under pressure water immersion. The results indicated that with an increase in the pressure water immersion duration, the average tensile strength of coal samples in Groups B to E decreased by 42.72%, 50.49%, 55.34%, and 60.19%, respectively, compared with those in Group A. The strain isopotential lines of the coal samples became progressively denser and converged toward the deformation localized zone of the main macro-tensile cracks. The increase in pressure water immersion duration intensified the water–coal rock interaction and disrupted the initial energy storage structure of the coal samples, resulting in a gradual reduction in their pre-peak energy storage capacity. Compared with Group A, the average energy storage capacity *(U)* of the coal samples in Groups B to E decreased by 50.26%, 68.91%, 76.68%, and 84.46%, respectively. With an increase in the pressure water immersion duration, compared with the A-1 coal samples, the rupture fracture of the B-1, C-1, D-1, and E-1 coal samples exhibited more microcracks, more pores, larger cavities, and looser particle arrangements. Additionally, their surfaces gradually became flocculent. The structure of the coal samples transformed from dense to loose and porous, enhancing the deterioration effect on their tensile properties.

Keywords: deformation damage; deterioration mechanism; energy evolution; microstructure characterization of rupture fracture; pressure water immersion duration

1. Introduction

As an important fossil fuel, coal occupies a pivotal position in China’s energy structure (Chen *et al.* 2018, Guo *et al.* 2023, Hua *et al.* 2015, Zhu *et al.* 2012). Mine water damage is an important factor that threatens the safe production of coal mines and causes many unfavorable hindrances to coal mining. The waterproof coal pillar—one of the important measures to prevent mine water damage accidents—has been eroded long-term by the accumulated water in the mined-out areas. Water‑coal rock interaction is the main cause of deformation and destruction of the waterproof coal pillar. Additionally, the destabilization of water-saturated coal pillars under load is mostly due to tensile damage (Hossein *et al.* 2018, Reed *et al.* 2017, Wong *et al.* 2016). Thus, for the rational design of coal pillars and ensuring their stability, it is important to study the tensile properties and deterioration mechanism of coal rock under erosion due to water accumulation in the mining area.

In recent years, researchers worldwide have investigated the tensile properties of coal and rock under the influence of water immersion. Song *et al.* (2020) investigated the effects of the water content and specimen size on the tensile strength of coal samples. Li *et al.* (2019) conducted tensile tests on saturated sandstone and found that water saturation reduced its dynamic tensile strength. Erguler *et al.* (2009) examined the effects of the water content on the tensile strength, elastic modulus, and tensile modulus of claystone. Song *et al.* (2023) performed tensile tests on sandstone with different water contents to study the effect of water on the sandstone tensile strength. Zhou *et al.* (2022) conducted tensile tests on sandstone with different water contents and examined the effect of the water content on its mechanical strength. Vasarhelyi *et al.* (2018) investigated the weakening effect of water on rock tensile strength and proposed a method for calculating the degree of weakening of the strength of water-bearing rocks. Yin *et al.* (2021) performed tensile tests on sandstone under different water immersion pressures and studied the effect of the water immersion pressure on its tensile properties. Yao *et al.* (2021) performed tensile tests on coal samples under different water contents and investigated the tensile strength of coal samples and their mechanical parameters as a function of water saturation. Huang *et al.* (2010) performed tensile tests on sandstone with different water contents and studied the rate dependence of tensile strength softening with different water contents. Cai *et al.* (2022) performed tensile tests on sandstone under different water contents and determined the relationship between the tensile strength and water content.

*Corresponding author, Professor
E-mail: 949251142@qq.com

ISSN: 2005-307X (Print), 2092-6219 (Online)

The above research results are important for understanding the tensile properties of coal and rock under the erosion of water accumulation in the mined-out area. In actual mining engineering, once a pressurized water environment is established in the mined-out areas, the waterproof coal pillars are subjected to prolonged immersion in pressurized water. However, the aforementioned studies mainly focused on the tensile properties of coal and rock with variations in the water content, immersion solution, and other factors, without considering the deterioration effects of pressure water immersion on the coal samples. In view of this, on the basis of previous research, a self-developed coal rock pressure water immersion test device was used in the present study to prepare dry coal samples and four sets of coal samples with different pressure water immersion durations (water immersion durations of 3, 6, 9, and 12 months, with an immersion pressure of 5 MPa). Using an XTDIC 3D full-field strain measurement system, a PoreMaster 33 mercury intrusion porosimeter, an X-ray fluorescence spectrometer, a laser ablation-inductively coupled plasma mass spectrometer, and an Apreo S Hivac high-resolution scanning electron microscope (SEM), Brazilian splitting tests were performed on the coal samples. The strength, deformation damage, and energy evolution characteristics of the coal samples were studied. By comparing macroscopic and microscopic structural observations, the mineral composition and pore structure were analyzed to investigate the tensile characteristics and deterioration mechanisms of the coal samples under different durations of pressure water immersion.

2. Sample preparation and test equipment

2.1 Sample preparation

The coal samples required for the test were collected from a coal mine in Shandong Province and analyzed using an X-ray diffractometer. The main mineral components identified were calcite (5.3%), illite (4.6%), quartz (4.5%), and kaolinite (9.7%), among others, as shown in Fig. 1.

To reduce the effect of coal sample dispersion on the experimental results, all the coal samples were collected from the same coal block. As shown in Fig. 2, the coal

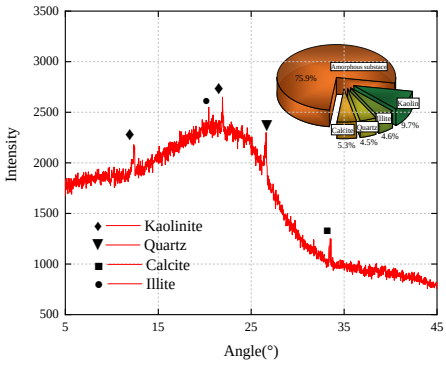

Fig. 1 XRD test results

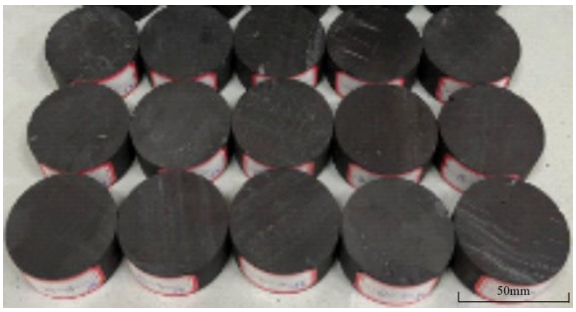

Fig. 2 Coal samples

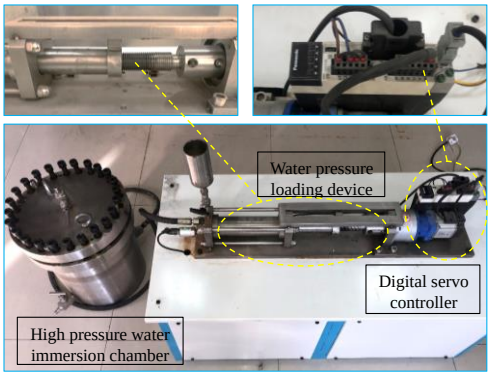

Fig. 3 Coal sample pressure water immersion test device (Yin 2023)

block was first drilled into a cylindrical sample with a diameter of 50 mm using a core drilling machine. This cylindrical sample was then cut into a disk-shaped specimen with a height of 25 mm using a stone sawing machine. Finally, both ends of the coal sample were smoothed with a stone grinding machine, ensuring that the two end surfaces non-parallelism was <0.05 mm and the diameter deviation was <0.02 mm (General Administration of Coal Science and Research 2009).

A total of 15 coal samples were processed and prepared. They were divided into five groups—A, B, C, D and E—with three in each group. As shown in Fig. 3, immersion treatment was performed on each group of coal samples using the self-developed coal rock pressure water immersion test device (Yin 2023). The coal samples in Group A were not subjected to immersion treatment (dry state). In contrast, the coal samples in Groups B to E were immersed in pressure water for durations of 3, 6, 9, and 12 months, respectively, with a constant immersion pressure of 5 MPa for all groups, The temperature and pH value of water in the process of pressure water immersion remain constant.

The coal rock pressure water immersion experimental device mainly consists of a high-pressure water immersion chamber, a servo booster cylinder, a pressure sensor, a digital servo controller, and an acquisition system. The high-pressure water immersion chamber is a cylindrical stainless steel container with an outer diameter of 300 mm and an inner diameter of 250 mm. Its top and upper pressure plate are reinforced with rubber rings to ensure a leak-proof seal for the pressurized water. The digital servo controller

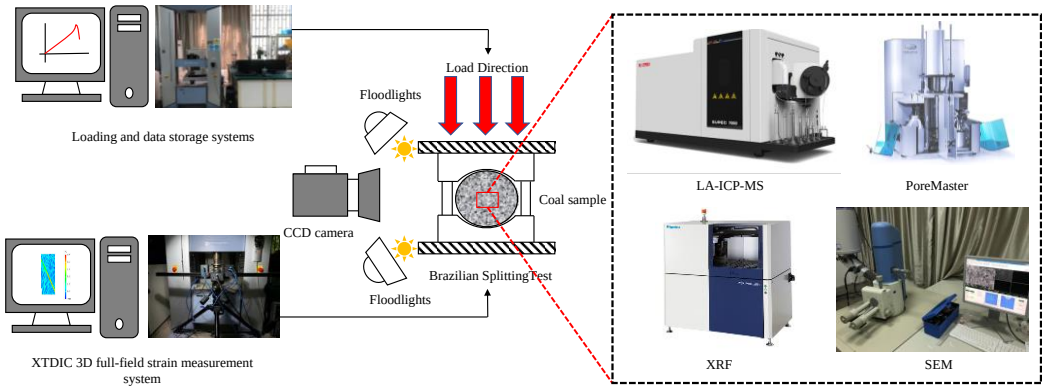

Fig. 4 Test control and monitoring system

includes a servo motor and a digital controller, with the servo motor connected to the pressurization transmission device. When filling and pressurizing, the command is edited by the operating software of the upper computer and sent to the digital servo controller. The controller then transmits the command to the servo motor, which, through the transmission device, pushes the piston in the pressurizing cylinder to fill and pressurize the high-pressure water immersion chamber. The pressure sensor is connected to the acquisition system for real-time monitoring. Once the target water pressure is reached, the termination command is fed back to the digital controller, and the servo motor stabilizes and maintains the pressure, forming a closed-loop control system.

2.2 Experimental systems

The main control and monitoring systems for this test included a loading system, the XTDIC 3D full-field strain measurement system, the PoreMaster 33 mercury intrusion porosimeter, the X-ray fluorescence spectrometer, the laser ablation-inductively coupled plasma mass spectrometer, and the Apreo S Hivac high-resolution SEM, as shown in Fig. 4.

The loading system was a Shimadzu AG-X250 electronic universal testing machine with a maximum load of 250 kN (Yin 2022), Loading rate is 0.07kN/s. The XTDIC 3D full-field strain measurement system mainly consisted of a CCD camera, an image acquisition card, a monitor, and a computer. The PoreMaster 33 mercury intrusion porosimeter was equipped with a single high-pressure station suitable for various sample configurations, with pore sizes ranging from 6.4 to 1100 nm. The ZSX Primus IV X-ray fluorescence spectrometer utilized a dual vacuum system, automatic vacuum control, mapping/micro-area analysis, high sensitivity for ultra-light elements, and automatic core cleaning. The laser ablation-inductively coupled plasma mass spectrometer used a COMPex 102 ArF laser with a working wavelength of 193 nm, a spot size on the sample ranging from 2 to 160 μm, and an optical resolution of 1 μm. An Apreo high-resolution SEM was used, with a resolution of 0.8 nm (15 kV) to 0.9 nm (500 V) and a standard magnification of 100–500,000×.

For the Brazilian splitting tests, the loading system and the strain measurement system were synchronized to ensure that the same time parameters were used for data processing and analysis (Ding 2023).

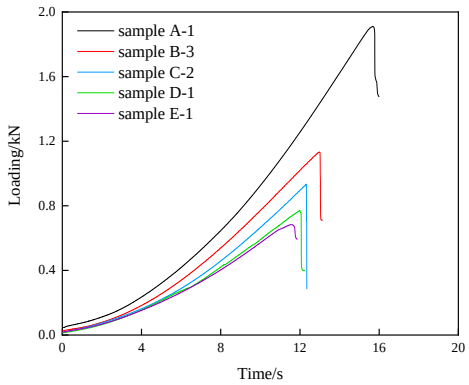

Fig. 5 Load–time curves of coal samples

3. Strength and deformation damage

3.1 Strength characteristics of coal samples

The load-time curves of coal samples under different pressure water immersion durations are shown in Fig. 5. The axial load-time curves of the coal samples under different pressure water immersion durations were essentially the same, and all of them went through three stages: compaction, elastic deformation, and post-peak drop. After the load of dry coal samples reached the peak tensile strength, it dropped abruptly to zero, exhibiting clear brittle failure characteristics. With an increase in the pressure water immersion duration, the compaction stage of the coal samples was prolonged. The plastic deformation stage of the E-1 coal samples in the splitting process was significantly longer and did not drop rapidly when the load reached its peak. The coal samples exhibited certain plastic damage characteristics. This indicated that under the effect of pressure water immersion, the coal samples underwent physical and chemical deterioration under water. The intermolecular forces within the particles decreased, reducing the brittleness and increasing the plasticity; thus, the coal samples had plastic softening characteristics.

Fig. 6 shows the comparison curves of tensile strength of coal samples under different pressure water immersion durations. The average tensile strength of the coal samples in Groups B to E were reduced by 42.72%, 50.49%, 55.34%, and 60.19%, respectively, compared with that of Group A coal samples. This is because with an increase in

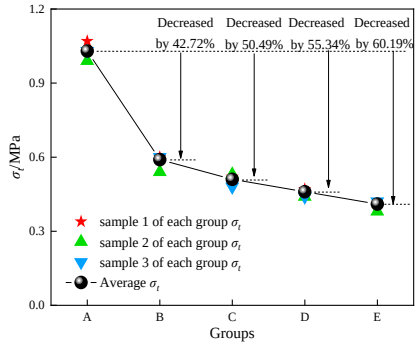

Fig. 6 Uniaxial tensile strengths of coal samples

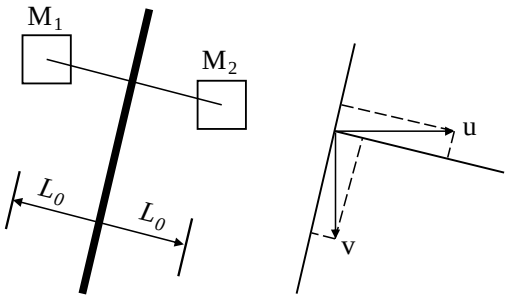

Fig. 7 Analytical method for the displacement evolution of the deformation localization band (Miao 2024)

the pressure water immersion time, the interaction between water and coal rock was enhanced, leading to the precipitation of hydrophilic clay minerals within the coal samples and a reduction in cohesion between particles. Additionally, this process promotes the expansion of macroscopic and microscopic cracks and reduces the friction difficulty along the macroscopic crack surfaces. This exacerbates the internal damage of the coal samples, weakens their solid load-bearing structure, and reduces the effective load-bearing area, corresponding to a decrease in tensile strength. However, with an increase in the water immersion time, when the hydrophilic clay minerals are completely dissolved, the dissolution effect of mine water on the coal sample particles becomes weaker, and the water-coal rock interaction slows. Consequently, the deterioration of the coal samples gradually weakens and tends to stabilize.

3.2 Deformation damage characteristics of coal samples

To study the macrocrack extension evolution law of the coal samples under different pressure water immersion durations, the deformation field evolution characteristics during Brazilian splitting tests of coal samples A-1, B-3, C-2, D-1, and E-1 were analyzed using the displacement dislocation momentum of the deformation localization band calculation method. First, the deformation localization band of the main strain contours before the final destruction of coal samples was divided, and then the analysis method for the displacement evolution on both sides of the deformation localization band proposed in the literature (Miao 2024) was used, as shown in Fig. 7. The displacement dislocation momentum of the deformation localization band of the five groups of coal samples was calculated (L_0 represents the distance of both sides of the marking line of the deformation localization zone, which is 2 mm). The points M_1 and M_2 are the centers of the selected pixel points. u and v are the displacement components of the selected pixel points). Finally, to facilitate the subsequent analysis, five characteristic points (a-e) on the load-time curves of the coal samples were selected to analyze the maximum principal strain field and displacement dislocation momentum evolution of the corresponding deformation field at the moment when the deformation field first begins to evolve.

Fig. 8 shows the evolution curves and contours of the displacement dislocation momentum in the localized zone of coal deformation in the Brazilian splitting test. From Fig. 8, it can be seen that at the early stage of loading (characteristic point b), the overall deformation of the coal samples is uniform, and the displacement dislocation momentum is in the stage of three micro-variations. With an increase in the load (characteristic point c), the A-1 coal sample first forms a deformation localization zone in the primary crack region and develops and expands along the direction of the maximum principal stress. The localization zones I-K begin to enter the growth stage and last for a long time, but owing to the formation of the localization zones and the expansion of the cracks, the growth rate of the displacement dislocat ion momentum is relatively different. Among them, localization zone K was formed by the main control crack that led to the final damage of the A-1 coal sample; thus, its displacement dislocation momentum growth rate was higher. The displacement dislocation momentum of localized zones of the B-3, C-2, and D-1 coal samples sequentially entered the growth stage, indicating that the increased duration of pressure water immersion enhanced the water-coal interaction and exacerbated the damage to the coal samples. A total of three deformation localization zones appeared in the E-1 and D-1 coal samples, indicating significant progressive internal destruction, which promoted crack displacement dislocation. Conversely, the C-2 and B-3 coal samples exhibited relatively minor progressive destruction, and the localization zones in the A-1 coal sample were the last to begin evolving. At the stress peak (characteristic point d), the primary and new cracks of each group of coal samples intersected and penetrated, with significant stress concentration at the macroscopic cracks that controlled the damage, resulting in a sudden increase in the displacement dislocation momentum in the localized zones. The coal samples were destroyed as a whole in the post-peak stage (characteristic point e), and the evolution of deformation localized zones was relatively intense. However, with an increase in the pressure water immersion time of the coal samples, the cracks were developed to a greater extent, and the relative misalignment between the cracks was significant, which led to increased fragmentation of the coal samples. Compared with the A-1 coal sample, the cracks in the B-3, C-2, D-1, and E-1 coal samples were fully extended, and the degree of fragmentation was drastic.

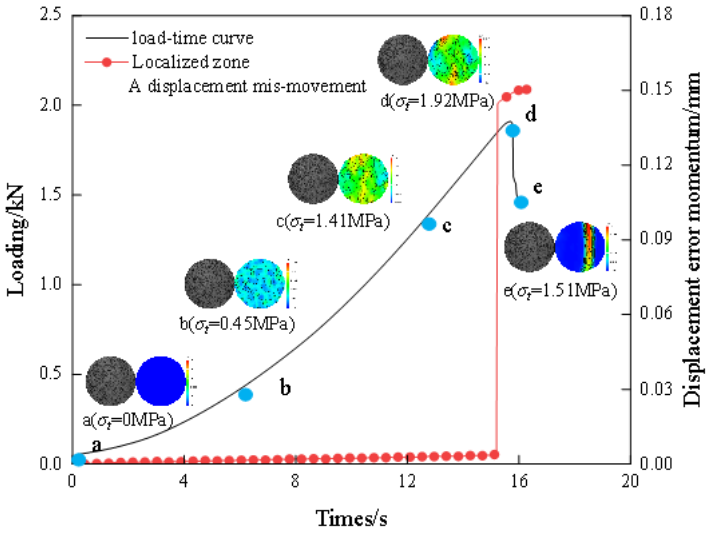

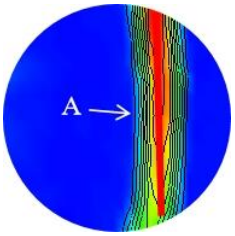

Localized zone division

(a) A-1

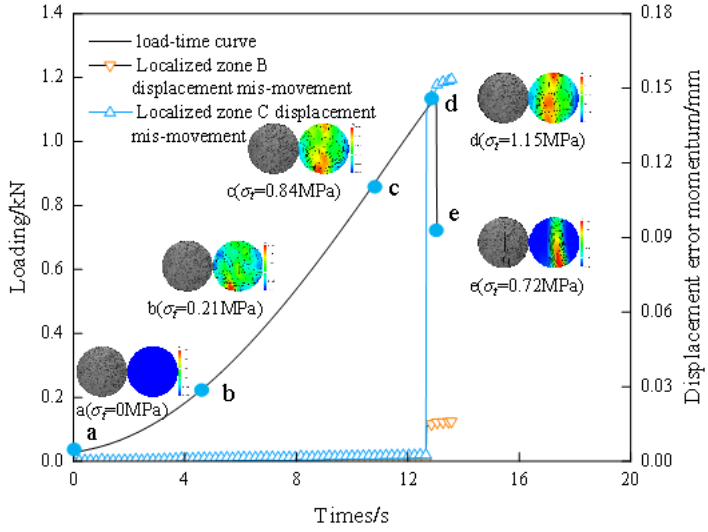

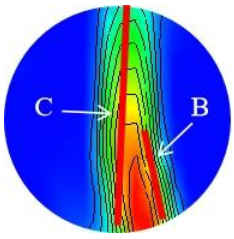

Localized zone division

(b) B-1

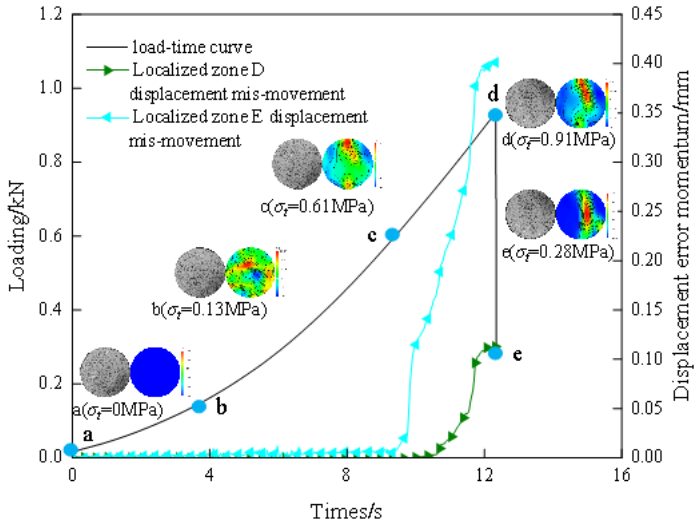

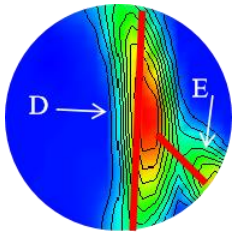

Localized zone division

(c) C-1

Fig. 8 Evolution curves and contours of displacement dislocation momentum in the localized zone of coal deformation in the Brazilian splitting test

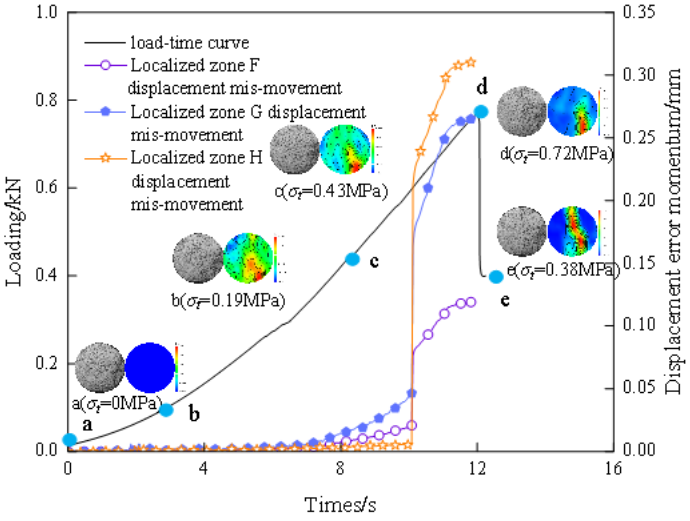

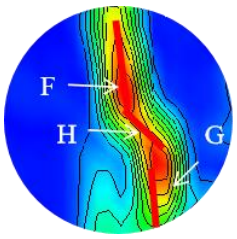

Localized zone division

(d) D-1

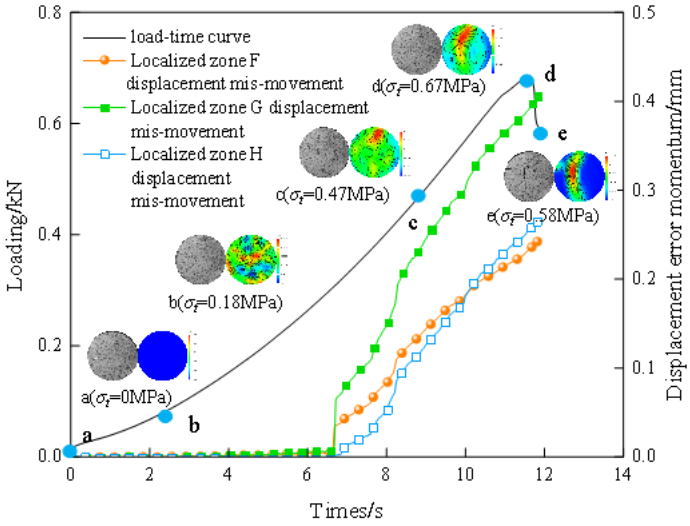

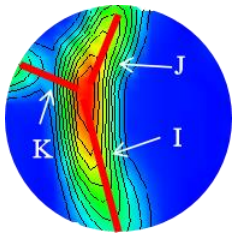

Localized zone division

(e) E-1

Fig. 8 Continued-

4. Pre-peak energy evolution law of coal samples

Coal sample deformation damage is an energy-driven state destabilization phenomenon. When the external input energy reaches the energy-storage limit of the coal sample, damage destabilization occurs. Therefore, in addition to the tensile strength, the magnitude of the stored energy before the peak of a coal sample is an important indicator of its ability to resist external perturbations. Compared with the tensile strength, the stored energy before the peak is a comprehensive reflection of the deformation damage of the coal sample, providing a more comprehensive and integrated indication of its ability to resist deformation damage. In the Brazilian splitting test, the deformation value of coal samples cannot be effectively obtained, which does not allow for the calculation of the pre-peak stored energy of coal samples.

According to the first law of thermodynamics, it is assumed that there is no heat exchange between the coal sample and the outside world when the external force does its work. In the pre-peak stage, part of the external input energy U is stored as elastic energy Ue inside the coal sample, and the other part is used as dissipated energy U_d for crack expansion and plastic deformation inside the coal sample. Therefore, on the basis of references (Xie 2005), the characteristics of coal sample pre-peak stored energy evolution were investigated by analyzing the change rule of U. Additionally, U can be considered as the mechanical energy applied to the coal sample by the testing machine, that is

$$U = \frac{1}{2} P_{\max} S \quad , \tag{1}$$

Where P_{max} represents the ultimate load of the coal sample, in kN, and S represents the axial displacement corresponding to the ultimate load, in mm.

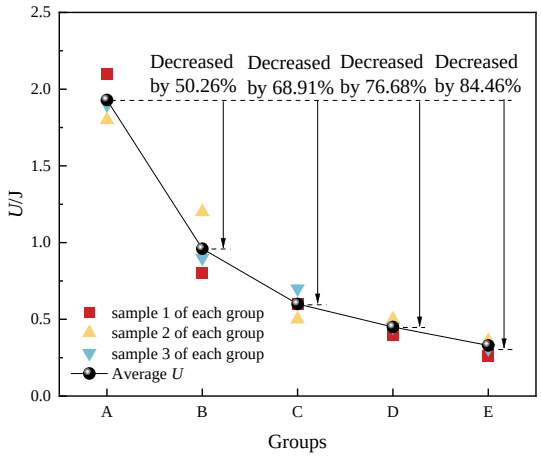

Fig. 9 *U*-value comparison of the coal samples

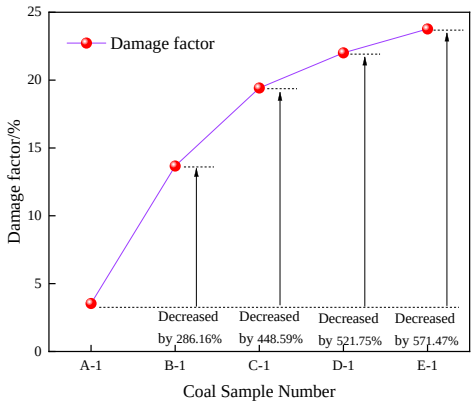

Fig. 10 Damage coefficients of coal samples under different pressure water immersion durations

Using Eq. (1), the stored energy U for each group of coal samples was calculated separately, as shown in Fig. 9. The Group A coal samples had the largest average U, i.e., 1.93 J, while the Group E coal samples had the smallest average U, i.e., 0.33 J. With an increase in the pressure water immersion time, the U of the coal samples decreased, which was consistent with the change rule of their tensile strength. Compared with the Group A coal samples, the average U of the Groups B, C, D, and E decreased by 50.26%, 68.91%, 76.68%, and 84.46%, respectively. This indicates that as the pressure water immersion duration increased, the capacity of coal samples to store energy before the peak decreased, leading to a corresponding reduction in their resistance to deformation damage. On one hand, the increase in water immersion time exacerbates the water–coal rock interaction, leading to greater initial damage within the coal samples, which forms a large number of microcracks, holes, and other defects, while destroying the initial energy-storage structure of the coal samples. On the other hand, as the load increases, the defects in the coal samples under the effect of pressure water immersion become more prone to stress concentration, which leads to the development and expansion of these defects. Additionally, primary macroscopic cracks are more likely to slide, causing secondary damage to the energy-storage structure of the coal samples, which results in their final destruction.

5. Coal sample deterioration mechanisms

5.1 Macrostructural analysis of coal samples

The damage factor is an index that characterizes the deterioration of the mechanical properties of a material subjected to a certain state of stress, which is typically related to the emergence and expansion of microcracks within the material, as well as the weakening of cohesive forces. Five coal samples—A-1, B-1, C-1, D-1, and E-1—were selected after different pressure water immersion durations. The end face images of the five samples were imported into ImageJ software for binarization. The threshold value was input into the Threshold tool and segmented into binarized images. The median filter was used to reduce the noise of the binarized images, where the white area represented the matrix, and the black area represented the cracks and pores. The "damage factor" D (Baud 2004) for each image was then calculated according to the built-in numerical value of the software, as follows

$$D = \frac{A_D}{A} \tag{2}$$

Where A_D represents the area of the black region in the binarized image, in mm^2; and A represents the total area of the binarized image, in mm^2.

The calculated damage coefficients of each coal sample are shown in Fig. 10. Fig. 11 presents the end face rupture of the disc coal sample and its binarized image under the influence of different pressure water immersion durations. In Figs. 10 and 11, it can be seen that the A-1 coal sample has better surface integrity and is relatively smooth, with an average damage coefficient of 3.54%. The B-1 coal sample has a long crack in the middle of the end face, and the end face is relatively flat, with an average damage coefficient of 13.67%. The C-1 coal sample is fractured at the corners, with an average damage coefficient of 19.42%. The D-1 coal sample exhibits more cracks on the end face, and the damage is further intensified, with an average damage coefficient of 22.01%. The E-1 coal sample has severe damage at the corners, with significant end face damage, numerous fine cracks and small holes, a large "pit," cracks extending along and through the joints, groups of fine cracks, a rough texture, and a small amount of coal debris within the cracks. The overall integrity of this sample is poor, with an average damage coefficient of 23.77%. With an increase in the pressure water immersion duration, the water–coal rock interaction was enhanced, and the damage coefficient of the coal sample end face increased.

In this uniaxial compression test of non-equal-size rock-coal composite specimens, one specimen was selected for each group to analyze the evolution characteristics of deformation field. Four feature points were taken to show the strain cloud diagram during the loading process, and the deformation and crack propagation process of the specimen were recorded and analyzed, as shown in Fig. 7 (feature

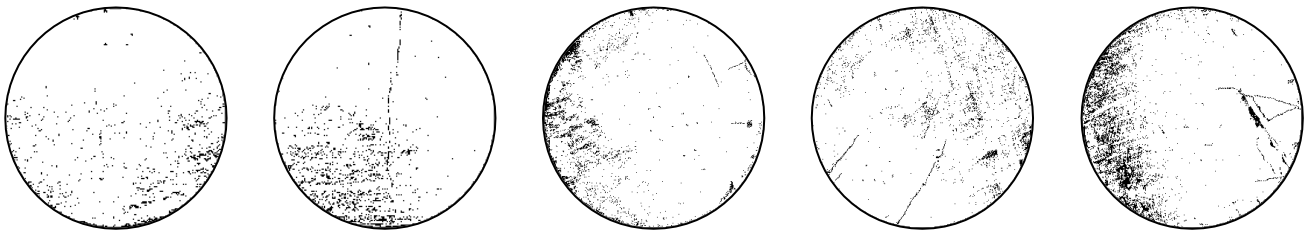

(a) A-1 (b) B-1 (c) C-1 (d) D-1 (e) E-1

Fig. 11 Disk coal samples' end faces and binarization images

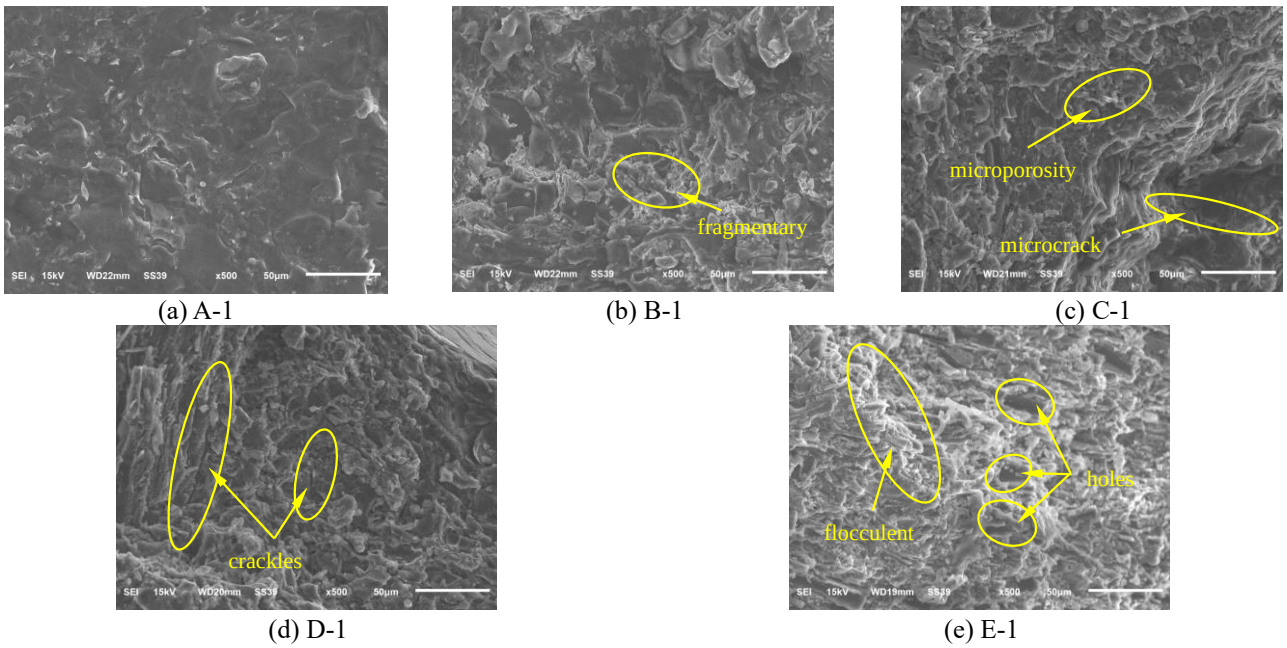

(a) A-1 (b) B-1 (c) C-1

(d) D-1 (e) E-1

Fig. 12 SEM images of coal sample rupture fracture under different pressure immersion durations

point a was selected in the initial state, and feature points b, c and d were respectively in the later stage of compaction stage, the middle stage of elastic deformation stage and the early stage of post-peak steep drop stage). Taking the scattering image of the specimen surface at the initial moment of loading as the reference standard, the scattering images obtained during the loading process were analyzed and processed by the digital image correlation method to obtain the cloud map of the strain field evolution of the surface of the non-equal-size rock-coal specimen under the uniaxial loading, which is shown in Fig. 8. Among them, the feature point a is the digital speckle correlation method to select the corresponding point of the reference image, the feature point b ~ d is the digital speckle correlation method to select the corresponding point of the deformed image, and P is the load corresponding to the feature point.

5.2 Microstructural analysis of coal samples

5.2.1 Coal sample rupture fracture morphology

SEM scans were performed on the fracture surfaces of the A-1, B-1, C-1, D-1, and E-1 coal samples to study their rupture fracture morphologies under different pressure water immersion durations, as shown in Fig. 12.

As shown in Fig. 12(a), the rupture fracture of the A-1 coal sample exhibited a dense structure with fewer cracks and pores and a smooth, angular surface. Owing to the relative internal integrity of the coal samples, the corresponding tensile strength is higher, and the interaction between water and coal increases. The hydrophilic clay minerals within the coal samples continue to soften, sludge, and dissolve, leading to the formation of microcracks and pores at the fractures. Compared with the A-1 coal samples, the fractures of the B-1, C-1, D-1, and E-1 samples exhibit more microcracks and pores, with larger holes and more loosely packed particles. Additionally, these samples exhibit a flocculent surface, indicating a transition in their structure from dense to loose and porous, as illustrated in Figs. 12(b)-12(e).

5.2.2 Microscopic characteristic parameters of coal samples

A Particle and Crack Analysis System (Liu *et al*. 2011) image recognition and analysis system is used to quantitatively analyze the pores and fractures of coal samples. The system can import a variety of pore images through binarization, automatically remove clutter, automatically segment and identify pores, output geometric and statistical parameters, and calculate the parameters of coal sample SEM image.

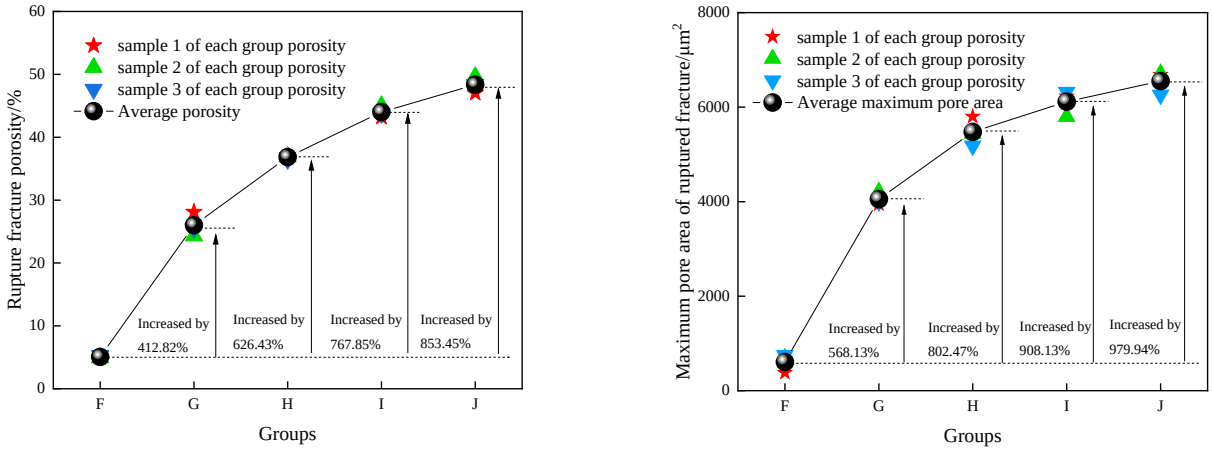

Fig. 13 Microscopic parameters of rupture fracture of coal samples under different pressure water immersion durations

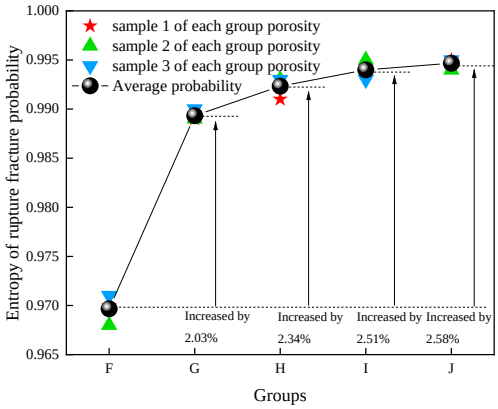

Fig. 14 Entropy of the coal sample rupture fracture probability

Probability entropy is an indicator that describes the directionality of pores; the porosity is automatically identified and calculated by the Particle and Crack Analysis System. The directionality parameter of microscopic pores in SEM images can be obtained using PCAS image analysis software. The probability entropy indicator ranges from 0 to 1. When the value of probability entropy is 0, all the pores in the image are oriented in the same direction, while when the value of probability entropy is 1, the directions of all the pores in the image are randomly distributed. The formula for calculating probability entropy is as follows

$$H_m = -\sum_{i=1}^{n} \frac{m_i}{M_1} \frac{\ln\left(\frac{m_i}{M_1}\right)}{\ln n} \tag{3}$$

Where H_m represents the probability entropy, m represents the number of intervals in the ith interval along the long axis direction of the pores, M_1 represents the total number of particles, and n represents the number of azimuthal zones equally divided in the direction of arrangement from 0° to 180° in units of 10°, with n = 18.

As shown in Fig. 13, the average porosity and the maximum area of the average pore at the rupture fracture are the smallest for the coal samples in Group A. With an increase in pressure water immersion time, both the average porosity and the maximum area of the average pore at the rupture fracture of coal samples in Groups B to E exhibit an increasing trend. Specifically, the average porosity and the maximum area of the average pore of coal samples in Group E have increased by 853.45% and 979.94%, respectively, compared to those in Group A. This is primarily attributed to the increase of water–coal rock interaction with the increase of pressure water immersion time, hydrophilic clay minerals within the coal samples can cause the expansion of the internal pores of the coal samples, cracks are more likely to expand through, resulting in an increase in both the number and area of pores at the rupture fracture of the coal samples. Therefore, its average porosity and maximum pore area increased accordingly. However, with the increase of time, its upward trend gradually slows down.

With an increase in the pressure water immersion time, the probability entropy of the pores at the rupture fractures of the coal samples exhibited an increasing trend. Compared with the Group A samples, the average probability entropy of the coal samples in Groups B to E increased by 2.03%, 2.34%, 2.51%, and 2.58%, respectively. This is because with an extended pressure water immersion time, the interaction between the water and coal rock was enhanced, leading to the formation of pore water pressure from the undischarged water. This weakened the adhesion between cemented particles, causing the roughness at the rupture fracture surface and resulting in deterioration of the pore orientation. Consequently, the probability entropy increases. However, as the pressure water immersion time continues to increase, the increase in pore probability entropy at the coal sample rupture fracture slows and eventually reaches a stable state.

5.3 Mineral composition analysis of coal samples

To investigate the change in the clay mineral content of coal samples after erosion by water accumulated in the mined-out areas, the mineral composition of each group of coal samples was analyzed using an X-ray diffractometer. The results are presented in Table 1.

Table 1 Quantitative analysis of mineral components using X-diffraction

Group	Mineral contents/ (%)			
	Quartz	Calcite	Elysium	China clay
A (dry)	5.3	4.5	4.6	9.6
B (3 m)	5.1	4.3	3.4	7.3
C (6 m)	5.0	4.0	2.6	6.5
D (9 m)	4.8	3.9	1.8	5.8
E (12 m)	4.5	3.8	1.3	5.0

Table 2 Normal ion concentration and pH of the solution

Group	pH	K^+ / (mg/L)	Na^+ / (mg/L)	Ca^{2+} / (mg/L)	Ae^{3+} / (mg/L)	Al^{3+} / (mg/L)	Cl^- / (mg/L)	SO_4^{2-} / (mg/L)	HCO_3^- / (mg/L)
A (dry)	6.41	4.76	729.85	22.62	1.24	25.98	96.24	1477.89	61.93
B (3 m)	7.28	7.53	958.50	24.18	1.56	26.73	96.34	1586.15	62.97
C (6 m)	7.32	8.10	967.63	25.62	1.71	26.91	96.36	1591.36	63.16
D (9 m)	7.35	8.23	989.65	26.79	1.89	26.99	96.42	1596.55	63.21
E (12 m)	7.35	8.30	1001.02	28.11	1.93	27.04	96.43	1601.37	63.23

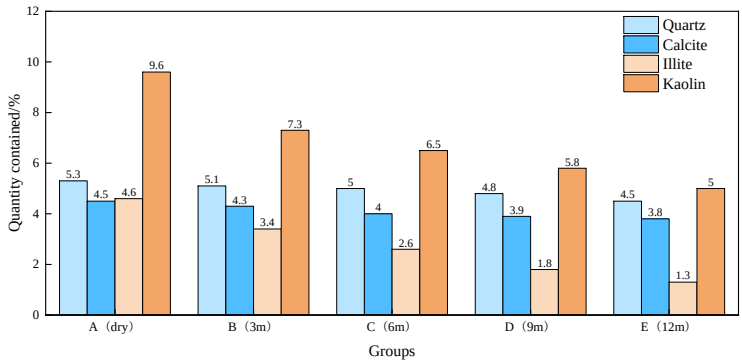

Fig. 15 Mineral composition changes

As shown in Fig. 15, with an increase in the pressure water immersion time, the contents of illite and kaolinite minerals in the coal samples of Groups A to E decreased. Compared with the coal samples from Group A, the illite and kaolinite contents in the coal samples from Group E decreased by 71.74% and 47.92%, respectively. This was due to the water–coal rock interaction after the immersion of coal samples. Some of the clay minerals (illite and kaolinite) were softened and muddied, and dissolved in the water, mixing with the mine water solution, which reduced their contents after immersion. As the duration of pressure water immersion increases, the water–coal rock interaction was exacerbated. However, the degradation of the coal samples by the mine water gradually slowed.

To investigate the hydrochemical reactions of coal samples with different durations of pressure water immersion, the concentration of conventional ions contained in the immersion solution as well as the pH of the solution were measured using laser ablation-inductively coupled plasma mass spectrometry and a pH meter. The concentration of conventional ions contained in the immersion solution, as well as the pH value of the solution, are presented in Table 2.

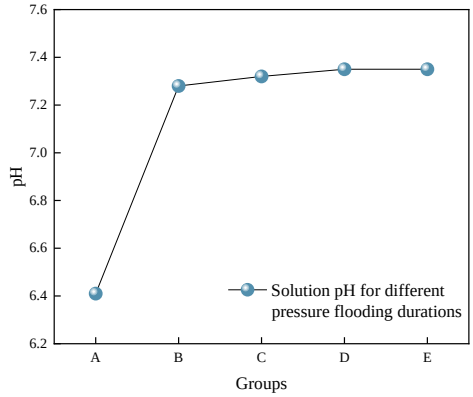

Fig. 16 pH values of coal samples soaked in an aqueous solution

As shown in Fig. 16, the initial pH value of the water accumulated in the mined-out area, which was used for the test, was 6.41, indicating an acidic solution. The test solution for Group A was the original water sample, while Groups B to E used the coal sample soaking solutions. The pH value of the soaking water solution rapidly increased to 7.28, and with an increase in the pressure water immersion

time, the pH value stabilized at approximately 7.35, indicating alkaline hydrochemical characteristics. From Table 3, this is mainly because when the coal samples were first immersed, the water accumulated in the mined-out area was acidic. Aluminosilicate minerals and hydrophilic clay minerals (such as illite and kaolinite) in the coal samples reacted rapidly with the H^+ in the solution via chemical reactions or with the water molecules in the immersed solution through ion exchange or hydrolysis, increasing the pH, as given by Eqs. (4)-(9), which increased the concentrations of Ca^{2+}, K^+, Al^{3+}, Ae^{3+}, and Na^+ in the immersion solution of the coal samples. With the increase in the pressure water immersion duration, the water–coal rock interaction was enhanced, accelerating chemical reactions, ion exchange, and hydrolysis reactions. However, owing to the spatial limitations of the container used for immersion, when most of the H^+ and water Reaction process of illite with water

$$K_{0.9}Al_{2.9}Si_{3.1}O_{10}(OH)_2 + nH_2O \longrightarrow K_{0.9}Al_{2.9}Si_{3.1}O_{10}(OH)_2 nH_2O \quad (4)$$

Reaction process of calcite with hydrogen ions

$$P20 = \frac{\text{Sum20}}{\text{n}} \times 100 \quad (5)$$

Reaction process of potassium feldspar with hydrogen ions

$$2KAlSi_3O_8 + 2H^+ + H_2O = Al_2Si_2O_5(OH)_4 + 4SiO_2 + 2K^+ \quad (6)$$

Reaction process of hematite with hydrogen ions

$$2KAlSi_3O_8 + 2H^+ + H_2O = Al_2Si_2O_5(OH)_4 + 4SiO_2 + 2K^+ \quad (7)$$

Reaction process of hematite with hydrogen ions

$$2KAlSi_3O_8 + 2H^+ + H_2O = Al_2Si_2O_5(OH)_4 + 4SiO_2 + 2K^+ \quad (8)$$

Reaction process of sodium feldspar with water:

$$2NaAlSi_3O_8 + 2H^+ + 9H_2O \longrightarrow Al_2Si_2O_5(OH)_4 + 2Na^+ + 4H_4SiO_4 \quad (9)$$

5.4 Pore structure analysis of coal samples

Porosity of coal samples is an important parameter for evaluating the degree of internal damage. Higher porosity indicates more microcracks and pores within the coal samples, a looser structure, and a lower bearing capacity. To quantitatively characterize the internal pore structure of the coal samples, the pore structures of the five groups of coal samples (A to E) were measured using the PoreMaster 33 mercury intrusion porosimeter. The results of the mercury intrusion test are presented in Table 3.

The average pore sizes, porosities, and median pore sizes of coal samples with different pressure water immersion durations are presented in Fig. 17. Compared with the coal samples of Group A, the average pore sizes, porosities, and median pore sizes of the coal samples of Groups B to E exhibited an increasing trend. This indicated that with the increase in the pressure water immersion duration, the water–coal rock interaction was enhanced. The clay minerals inside the coal samples softened, dissolved, and eroded, leading to the formation of new microcracks and pores, which increased the average pore size and porosity of the coal samples.

Fig. 18 shows the mercury inflow curves of the A-1, B-1, C-1, D-1, and E-1 coal samples, which were used to analyze the pore characteristics of the coal samples with different pressure water immersion durations. According to the Hodot

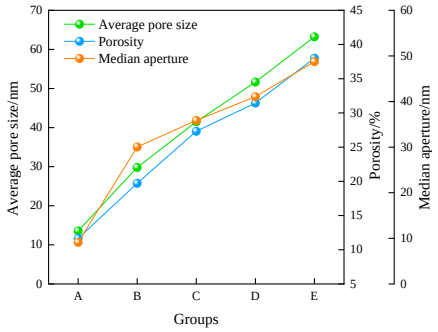

Fig. 17 Relationship between pore characteristics of coal samples

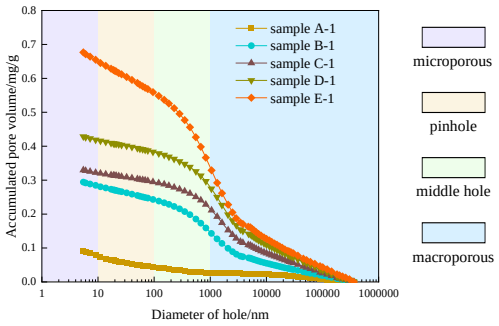

Fig. 18 Mercury inflow curves of coal samples

scheme (Hodot 1966), the pore spaces obtained from the mercury intrusion porosimetry test were divided into four types according to pore size: micropores (3–10 nm), pinholes (10–100 nm), middle holes (100–1000 nm), and macropores (>1000 nm). The curve reflects the degree of pore development at each pore size; a steeper curve corresponds to a larger pore-volume increment. The curve shapes exhibit significant differences.

In Fig. 18, the mercury inflow curves of the B-1, C-1, D-1, and E-1 coal samples all have an S-shape, and the mercury feed curves of the A-1 coal samples have an inverse S-shape. This indicates that for the A-1 coal samples, the micropores and macropores were the most developed, followed by the pinholes, with the middle holes being the least developed. The pore sizes of the A-1 coal samples were smaller than those of the B-1, C-1, D-1, and E-1 coal samples. Moreover, pores of various sizes gradually increase with the increase in the pressure water immersion time. This indicates that with the increase in the pressure water immersion time, the water–coal rock interaction is enhanced, altering the internal structure of the coal samples and exacerbating their damage. The internal pore size of coal samples gradually transitions from microporous, to pinhole, to middle hole, and finally to macroporous, which verifies to a certain extent the experimental conclusion that the porosity of the coal samples is positively correlated with the pressure water immersion time.

5.5 Deterioration mechanism of tensile properties of coal samples

Coal, as a discontinuous, homogeneous, and anisotropic special rock, develops defects such as primary cracks and pores. To further explore the macroscopic and microscopic

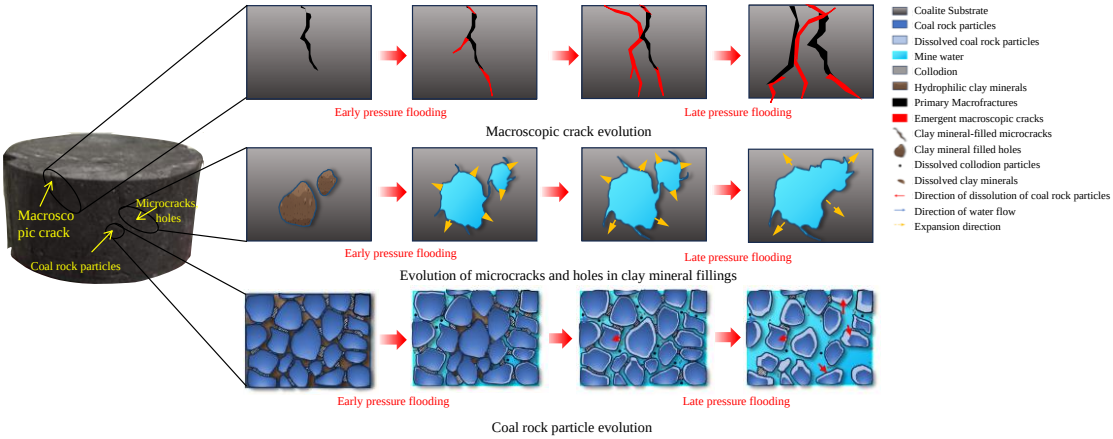

Fig. 19 Schematic of the damage evolution process of coal samples

deterioration mechanisms of the tensile properties of the coal samples under pressure water immersion in mined-out areas, a schematic of the damage evolution process of coal samples under such conditions was drawn. This process is divided into three stages: the dry state, early pressure flooding, and late pressure flooding, as shown in Fig. 19. It is assumed that the initial coal samples contain primary defects such as macrocracks, microcracks and holes, that the coal particles are in contact with each other and independent of each other, that they are bonded by cement, and that the defects of the coal samples are filled with hydrophilic clay minerals supplemented by a solid bearing structure to carry the pressure.

In the dry state, the coal samples exhibit good integrity. The structures of primary macroscopic cracks, microcracks, and holes are stable and few in number. The particles of the coal samples are primarily linked by cementing materials, with internal defects evenly distributed and filled by clay minerals, resulting in a dense structure. In the early pressure flooding, water molecules infiltrate the interior of coal samples through pore cracks and are adsorbed on the clay minerals and cement, which promotes the water–coal rock interaction, leading to the expansion of macroscopic cracks and microcracks. Part of the hydrophilic clay minerals and cementing materials in the holes and pores soften, sludge, and dissolve, reducing the adhesion force between the particles of the coal samples, hollowing out of the internal pores of the coal sample to form damage, and expanding holes and pores. The solid bearing structure of the coal sample is weakened, reducing its effective bearing structure area. In the late pressure flooding, as the clay minerals continue to dissolve, the cement is dislodged, leading to faster infiltration of water molecules. As a result, the number of microcracks and pores inside the coal samples increases significantly, increasing the porosity of the coal samples. The non-connected primary cracks are connected under the dissolution and erosion of the water to form new macroscopic cracks and microcracks, and the pores and the pores are expanded again. The lubrication effect of the water reduces the coefficient of friction of the primary closed cracks inside the coal samples, and the relative sliding difficulty of the crack surface decreases. This results in a further increase in internal defects, weakening the solid load-bearing structure of the coal samples and further reducing the area of the effective load-bearing structure. As the water immersion time increases, the internal hydrophilic clay minerals and cementing materials are completely dislodged, but the softening and dissolution effect on the coal sample particles is limited; thus, the deterioration degree of the coal samples decreases accordingly.

Therefore, with an increase in the pressure water immersion duration in the mined-out areas, the internal damage defects of coal samples gradually increase, and their physical bearing structure is continuously weakened. Under the load, larger internal defects of coal samples correspond to a smaller area of the effective bearing structure and a corresponding decrease in the tensile strength of the coal samples, with significant plastic deformation occurring before the peak stage. Additionally, owing to the undischarged water at internal defects forming pore water pressure, the driving force for the emergence and expansion of macrocracks, microcracks, and holes in the region is enhanced. Consequently, the degree of fragmentation of coal samples under load is increased, making deformation damage more likely to occur.

6. Conclusions

(1) As the duration of pressure water immersion increased, the tensile strength of the coal samples decreased. Specifically, the average tensile strength of the coal samples in Groups B to E decreased by 42.72%, 50.49%, 55.34%, and 60.19%, respectively, compared with the samples in Group A. The distribution of the maximum principal strain field in the coal samples was almost irregular. As the duration of pressure water immersion increased, the strain isopotential lines of the coal samples became progressively denser. Under loading, stress concentrations initially developed at primary macroscopic cracks, leading to the formation of localized deformation zones. With an increase in the pressure water immersion time, multiple localized deformation zones coalesced to form macroscopic main cracks. This resulted in a sudden increase in the displacement dislocation momentum at the peak stress, ultimately leading to intensified crushing of the coal samples.

(2) During the damage process, the elastic energy stored in the solid bearing structure of the coal samples decreased with

an increase in the pressure water immersion duration. Additionally, the energy-storage limit of the solid bearing structure of the coal samples decreased, and more external input energy was used for the macroscopic and microscopic damage in plastic intervals of the coal samples. Additionally, as the pressure water immersion duration of the coal samples increased, the released energy used for the coalescence and penetration of macrocracks in the coal samples increased.

(3) With the increase in the pressure water immersion time, the water–coal rock interaction was enhanced.

Additionally, the clay minerals were softened and muddied and dissolved, and new pores, microcracks, and macroscopic cracks evolved. This resulted in larger defects within the coal samples, weakened the solid bearing structure of the coal samples, reduced the effective bearing area of the samples, and reduced the strength of the samples and degraded the tensile properties accordingly. However, after a period of time, when the hydrophilic clay minerals were completely dissolved, the erosion of coal sample particles by the water accumulated in the mined-out areas slowed, decelerating the deterioration of the coal samples.

Acknowledgements

This work was supported by the National Natural Science Foundation of China (Grant Nos. 52274128), and the Open Fund Research Project, supported by the State Key Laboratory of Mining Response and Disaster Prevention and Control in Deep Coal Mines (Grant No. SKLMRDPC22KF01). This work was supported by the Taishan Scholars Project Special Fund (NO.tsqn202306199).

References

Baud, P., Klein, E. and Wong, T. (2004), "Compaction localization in porous sandstone: Spatial evolution of damage and acoustic emission activity", *Struct. Geol*., **26**(4), 603-624. https://doi.org/10.1016/j.jsg.2003.09.002.

Cai, X., Cheng, C.Q., Zhao, Y., Zhou, Z. and Wang, S. (2022), "The role of water content in rate dependence of tensile strength of a fine-grained sandstone", *Arch. Civil Mech. Eng*., **22**(1). https://doi.org/10.1007/s43452-022-00379-8.

Chen, S.J., Qu, X., Yin, D.W., Liu, X.Q., Ma, H.F. and Wang, H.Y. (2018), "Investigation lateral deformation and failure characteristics of strip coal pillar in deep mining", *Geomech. Eng*., **14**(5), 421-428. https://doi.org/10.12989/gae.2018.14.5.421.

Ding, Y.S., Yin, D., Hu, H., et al. (2023), "Influence characteristics and macro-meso mechanism of pressure immersion time on tensile properties for coal materials", *J. Mater. Res. Technol*., **26**, 2358-2370. https://doi.org/10.1016/j.jmrt.2023.08.030.

Erguler, Z.A. and Ulusay, R. (2009), "Water-induced variations in mechanical properties of clay-bearing rocks", *Int. J. Rock Mech. Min. Sci*., **46**, 355-370. https://doi.org/10.1016/j.ijrmms.2008.07.002.

General Administration of Coal Science and Research (2009), GB/T 23561 Methods for determining the physical and mechanical properties of coal and rocks, China Standard Publishing House.

Guo, X.P., Yang, L., Sun, X.S., Zuo, X.P. and Zhang, M. (2023), "Experimental study on deterioration law of tensile strength of dolomite under long term immersion", *J. China Three Gorges University (Natural Sciences)*, **45**(4), 19-24. (in Chinese) https://doi.org/10.13393/j.cnki.issn.1672-948x.2023.04.004.

Hodot, B.B. (1966), Outburst of Coal and Coal Bed Gas(Chinese Translation), China Coal Industry Press, Beijing, China, 18-33.

Hua, W., Dong, S.M., Li, Y.F., Xu, J.G. and Wang, Q.Y. (2015), "The influence of cyclic wetting and drying on the fracture toughness of sandstone", *Int. J. Rock Mech. Min. Sci*., **78**, 331-335. https://doi.org/10.1016/j.ijrmms.2015.06.010.

Huang, S., Xia, K., Yan, F. and Feng, X. (2010), "An experimental study of the rate dependence of tensile strength softening of Longyou sandstone", *Rock Mech. Rock Eng*., **43**(6), 677-683. https://doi.org/10.1007/S00603-010-0083-8.

Li, M., Lin, G., Zhou, W., Mao, X., Zhang, L. and Mao, R. (2019), "Experimental study on dynamic tensile failure of sandstone specimens with different water contents", *Shock Vib*., https://doi.org/10.1155/2019/7012752.

Liu, C., Shi, B., Zhou, J. and Tang, C.S. (2011), "Quantification and characterization of microporosity by image processing, geometric measurement and statistical methods: Application on SEM images of clay materials", *Appl. Clay Sci*., **54**(1), 97-106. https://doi.org/10.1016/j.clay.2011.07.022.

Masoumi, H., Roshan, H., Hedayat, A. and Hagan, P.C. (2018), "Scale-size dependency of intact rock under point-load and indirect tensile Brazilian testing", *Int. J. Geomech*., **18**(3). https://doi.org/10.1061/(ASCE)GM.1943-5622.0001103.

Reed, G., Mctyer, K. and Frith, R. (2017), "An assessment of coal pillar system stability criteria based on a mechanistic evaluation of the interaction between coal pillars and the overburden", *Int. J. Min. Sci. Technol*., **1**(27), 11-17. https://doi.org/10.1016/j.ijmst.2016.09.031.

Song, H., Li, S., Xu, J., Zhang, Q. and Zhi, Y. (2023), "Fractal characteristics and acoustic emission during the failure process of argillaceous siltstone with different moisture contents", *Geofluids*, https://doi.org/10.1155/2023/4558171.

Song, H.H., Zhao, Y.X., Jiang, Y.D. and Du, W. (2020), "Experimental investigation on the tensile strength of coal: consideration of the specimen size and water content", *Energies*, **13**(24). https://doi.org/10.3390/en13246585.

Miao, L.G., Niu, Y.Y., Shi, B.M. and Pan, Y. (2024), "Experimental investigation into dynamic damage mechanism of rockcoal-rock combinations based on digital image correlation method", *Acta Geodynamica ET Geomaterialia*, **21**(01), 71-82. https://doi.org/10.13168/AGG.2024.0006.

Vasarhelyi, B. and Davarpanah, M. (2018), "Influence of water content on the mechanical parameters of the intact rock and rock mass", *Eng. Geol*., **62**(4), 1060-1066. https://doi.org/10.3311/PPci.12173.

Wong, L., Maruvanchery, V. and Liu, G. (2016), "Water effects on rock strength and stiffness degradation", *Acta Geotechnica*, **11**(4), 713-737. https://doi.org/10.1007/s11440-015-0407-7.

Yao, Q.L., Wang, W.N., Li, X.H., *et al*. (2021), "Study of mechanical properties and acoustic emission characteristics of coal measures under water-rock interaction", *J. China Univ. Min. Technol*., **50**(3), 558-569. https://doi.org/10.13247/j.cnki.jcumt.001288.

Yin, D., Chen, S., Chen, B., Liu, R. and Li, F. (2021), "Experimental study on immersion effects of pressure water on the tensile characteristics of sandstone samples", *Geofluids*,. https://doi.org/10.1155/2021/6694881.

Yin, D., Ding, Y., Jiang, N., Li, F., Zhang, J., Xu, H. and Xu, X. (2022), "Mechanical properties and damage characteristics of coal samples under water immersion pressure", *Lithosphere*, https://doi.org/10.2113/2022/1278783.

Yin, D., Ding, Y.S., Wang, F., *et al*. (2023), "Experimental study on mechanical properties of pressure waterlogged coal rock

considering initial damage", *J. China Coal Soc*., **48**(12), 4417-4432. https://doi.org/10.13225/j.cnki.jccs.2023.0256.

Zhu, M., Deng, H.F., Zhou, S., Luo, Q. snf Cai, J. (2012), "Experimental research on fracture toughness and tensile strength of sandstone under water-rock interaction", *J. China Three Gorges University (Natural Sciences)*, **34**(5), 34-38+51+3+7. (in Chinese)

Zhou, K., Dou, L., Gong, S., Chai, Y., Li, J., Ma, X. and Song, S. (2022), "Mechanical behavior of sandstones under water-rock interactions", *Geomech. Eng*., **29**(6), 627-643. https://doi.org/10.12989/gae.2022.29.6.627.